MNRAS **467,** 1287–1293 (2017)
Advance Access publication 2017 January 24
doi:10.1093/mnras/stx186

Using photoionization models to derive carbon and oxygen gas-phase abundances in the rest UV

Enrique Pérez-Montero[1]★ and Ricardo Amorín[2,3,4]★

[1] *Instituto de Astrofísica de Andalucía, CSIC, Apartado de correos 3004, E-18080 Granada, Spain*
[2] *INAF–Osservatorio Astronomico di Roma, via di Frascati 33, I-00078 Monte Porzio Catone, Italy*
[3] *Cavendish Laboratory, University of Cambridge, 19 JJ Thomson Avenue, Cambridge CB3 0HE, UK*
[4] *Kavli Institute for Cosmology, University of Cambridge, Madingley Road, Cambridge CB3 0HA, UK*

Accepted 2017 January 19. Received 2017 January 16; in original form 2016 September 14

ABSTRACT

We present a new method to derive oxygen and carbon abundances using the ultraviolet (UV) lines emitted by the gas phase ionized by massive stars. The method is based on the comparison of the nebular emission-line ratios with those predicted by a large grid of photoionization models. Given the large dispersion in the O/H–C/O plane, our method first fixes C/O using ratios of appropriate emission lines and, in a second step, calculates O/H and the ionization parameter from carbon lines in the UV. We find abundances totally consistent with those provided by the direct method when we apply this method to a sample of objects with an empirical determination of the electron temperature using optical emission lines. The proposed methodology appears as a powerful tool for systematic studies of nebular abundances in star-forming galaxies at high redshift.

Key words: methods: data analysis – ISM: abundances – galaxies: abundances.

1 INTRODUCTION

Establishing the gas-phase abundances of carbon, nitrogen and oxygen in galaxies through cosmic time is key to understand not only their chemical enrichment, but also how galaxies assemble and evolve (Edmunds & Pagel 1978; Garnett et al. 1995; Henry, Edmunds & Köppen 2000; Chiappini, Romano & Matteucci 2003).

In the last decade or so, large deep optical spectroscopic surveys using ground-based 8–10-m class telescopes (e.g. Shapley et al. 2003; Steidel et al. 2003; Lilly et al. 2007; Kurk et al. 2013; Le Fèvre et al. 2015) led to a significant increase in the amount and depth of rest-frame ultraviolet (UV) spectra of high-redshift galaxies ($z \gtrsim 1$–2). These and other follow-up spectroscopy of galaxies in deep fields (e.g. Erb et al. 2010; Karman et al. 2015; Contini et al. 2016), in particular gravitationally lensed systems (e.g. Christensen et al. 2012; James et al. 2014; Stark et al. 2014; Vanzella et al. 2016a), are pushing now UV studies towards the low-luminosity (mass) regime out to redshift $z \sim 3.5$ (e.g. Patrício et al. 2016; Vanzella et al. 2016b, 2017; Amorín et al. 2017) and beyond (Stark et al. 2017, and references therein).

Overall, the above studies consistently find that the UV spectrum of high-redshift galaxies is systematically bluer and harder than in most local galaxies. Thus, it includes a number of high ionization, metal emission lines with relative large equivalent widths (EWs), such as those of carbon (e.g. C III] 1908 Å, C IV 1549 Å) and oxygen (O III] 1664 Å), which are often related to the presence of high equivalent width emission of He II 1640 Å and Lyα. While these spectral features could be quite common at very high redshifts (Stark et al. 2017), they provide tight constraints to the ionization, age and metallicity properties of galaxies, as recently shown by emission-line diagnostics based on detailed photoionization models (e.g. Feltre, Charlot & Gutkin 2016; Gutkin, Charlot & Bruzual 2016; Jaskot & Ravindranath 2016).

The wealth of information contained in the UV spectra of strong emission-line galaxies allows us to explore new techniques for an accurate characterization of the nebular chemical content of star-forming galaxies based on the analysis of the carbon abundance, the processes governing the C/O ratio and its relation with the total metallicity (e.g. Henry et al. 2000; Erb et al. 2010; Berg et al. 2016). The use of photoionization models assuming different combinations of C/O and O/H in an emitting ionized gas distribution is hence an alternative to estimate the gas-phase metallicity in those cases where very few UV emission lines can be measured. These methodologies, entirely or partially based on the available UV emission line ratios, are necessary to complement the widely used recipes to derive physical properties and chemical abundances from rest-frame optical spectra, which at $z \sim 2$–3 rely on the (usually challenging) detection of faint emission lines in the near infrared (e.g. Amorín et al. 2014; Maseda et al. 2014; Steidel et al. 2014; Troncoso et al. 2014; Shapley et al. 2015; Onodera et al. 2016; Sanders et al. 2016; Trainor et al. 2016). They would also be of great interest for metallicity studies of galaxies at the highest redshifts, where observing the optical rest frame is extremely challenging. In particular, the future arrival of unprecedentedly deep observations using the *James Webb Space Telescope* (*JWST*) and the new generation of 30-m class

★ E-mail: epm@iaa.es (EP-M); ra518@mrao.cam.ac.uk (RA)

telescopes, will increase by a huge factor current galaxy samples at $z \gtrsim 3$, extending detailed UV spectroscopic studies towards the cosmic dawn.

For this aim, in this paper we present an adapted version of the code HII-CHI-MISTRY (Pérez-Montero 2014, hereinafter HCM), originally designed to derive O/H and N/O from optical emission lines, that deals with UV emission lines to derive O/H and C/O ratios. This new semi-empirical method is fully consistent with direct estimations based on the electron temperature of star-forming regions and provide a potentially powerful tool to constrain the metallicity of galaxies out to very high redshifts. Even considering the inherent limitations affecting all methods for estimating chemical abundances in galaxies from their integrated spectra, such as, e.g. the fact that these are based on spatially unresolved data (e.g. Iglesias-Páramo et al. 2016) and rely on the simplistic assumption of a single H II region for the analysis of the observed emission lines, it is still possible to find characteristic abundance ratios (i.e. O/H, N/O, Pérez-Montero et al. 2016) that correlate with the integrated properties of galaxies, such as stellar mass, thus providing useful constraints for their assembly histories and chemical evolution.

Our paper is organized as follows; in Section 2, we describe the sample of objects with available emission lines both in the optical and in the UV whose O and C abundances could be derived using the direct method. In Section 3, we describe the models and the method used to derive the abundances and we compare our results with the direct abundances. Finally, in Section 4 we present our results and in Section 5 we summarize our conclusions.

Throughout this paper, the following convention is adopted: O/H is 12+log(O/H), C/O is log(C/O), O III] λ 1664 Å represents the total flux of 1661 and 1666 Å, C III] λ 1908 Å represents the total flux of lines at 1907 and 1909 Å, and C IV λ 1549 Å represents the total flux of lines at 1548 and 1551 Å.

2 CALIBRATION SAMPLE AND ABUNDANCES

We compiled from the literature a sample of H II regions and starburst galaxies at different z with optical and UV lines emitted by the gas ionized by episodes of massive star formation. Owing to the scarce number of objects with simultaneous measurement of optical and UV lines, our sample consists on a combination of integrated spectra observed using a variety of instruments and techniques. Our sample was selected in such a way that the O/H and C/O abundance ratios could be derived using the direct method from the estimation of the [O III] electron temperature, t_e([O III]). This was obtained from the ratio between [O III] 5007 and 4363 Å and, in some cases, from the ratio between [O III] 5007 and 1664 Å. Our calibration sample includes objects without observed fluxes in the [O II] 3727 Å line. For these objects, the total oxygen abundance was derived by applying an empirical calibration between O/H and t_e([O III]) (see below). For C/O determinations using the direct method, we compiled objects with measurements of at least O III] 1664 Å and C III] 1909 Å, and also C IV1549 Å in very high excitation objects. All the compiled fluxes were reddening corrected using a Cardelli, Clayton & Mathis (1989) extinction law based on the extinction coefficients given in these references. The list of references and the number of objects are listed in Table 1.

We recalculated the physical properties and the chemical abundances of the selected objects using expressions based on the PYNEB software (Luridiana, Morisset & Shaw 2012). The O/H abundances were calculated using the derived electron temperatures and the bright optical emission lines [O II] 3727 Å and [O III] 4959,5007 Å and the expressions given in Pérez-Montero (2014). In those cases, where the flux of the [O II] 3727 Å line were not available to calculate the O^+ abundances, we resorted to the empirical relation between O/H and t_e([O III]) given by Amorín et al. (2015), which is valid for a wide range of metallicity and ionization values.

Table 1. References and number of H II regions, local starbursts (LSB) and Lyman-break galaxies (LBG) used in this work.

Reference	Number of objects	Type
de Barros et al. (2016)	1	LBG
Bayliss et al. (2014)	1	LBG
Berg et al. (2016)	7	LSB
Christensen et al. (2012)	3	LBG
Erb et al. (2010)	1	LBG
Garnett et al. (1995)	6	LSB
Garnett et al. (1997)	2	LSB
Garnett et al. (1999)	6	H II
Izotov et al. (1999)	3	LSB
James et al. (2014)	1	LBG
Kurt et al. (1995)	2	H II
Kobulnicky et al. (1997)	3	LSB
Kobulnicky & Skillman (1998)	3	LSB
Steidel et al. (2016)	1 (stack)	LBG
Thuan, Izotov & Foltz (1999)	1	LSB
Vanzella et al. (2016a)	1	LBG
Villar-Martín, Cerviño & González Delgado (2004)	1	LBG

Using the PYNEB code, we also defined expressions for the temperature and carbon abundances using UV emission lines. Computing the emission line ratio:

$$R_{O3} = \frac{I(5007\ \text{Å})}{I(1664\ \text{Å})}, \tag{1}$$

we derive the [O III] electron temperature using the same set of atomic parameters as in Pérez-Montero (2014):

$$t_e([\text{O III}]) = 1.9263 + 6.43310^{-5} R_{O3} - 0.4221 \log(R_{O3}) \tag{2}$$

valid in the range t_e([O III]) = 0.8–2.5 in units of 10^4 K and that is nearly independent on electron density (i.e. a change from 10 to 1000 cm^{-3} implies a change in t_e of less than 0.1 per cent). Nevertheless, due to the very long wavelength baseline between the involved emission lines and the large extinction correction in the UV, the used ratio has a large uncertainty if the extinction correction is big. For instance, assuming an extinction of 1 mag at 1664 Å implies an electron temperature of about 10 per cent larger using a Calzetti et al. (2000) than a Cardelli et al. (1989) extinction law.

The carbon ionic ratios based on UV lines were derived using the following expressions and assuming the derived t_e[O III]:

$$\log(C^{2+}/O^{2+}) = \log\left(\frac{\text{C III] 1908 Å}}{\text{O III] 1664 Å}}\right) - 0.8361 - \frac{0.4801}{t_e} - 0.0358 t_e + 0.2535 \log(t_e) \tag{3}$$

$$\log(C^{3+}/O^{2+}) = \log\left(\frac{\text{C IV1549 Å}}{\text{O III] 1664 Å}}\right) - 1.5625 + \frac{0.2946}{t_e} - 0.043 t_e + 0.31 \log(t_e) \tag{4}$$

and using the collisional coefficients of Berrington et al. (1985) and Aggarwald & Keenan (2004) for C^{2+} and C^{3+}, respectively.

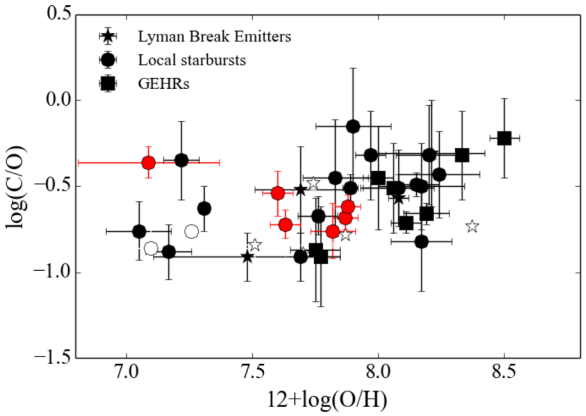

Figure 1. Relation between O/H and C/O for the studied sample as derived from the direct method. Different symbols stand for the class of objects and colours for the method used to derive abundances: direct method with 5007/4363 ratio (black), O/H from empirical relation with t_e[O III](red) and direct method using temperature from 5007/1664 ratio (white).

The total C/O was then derived under the assumption that

$$\frac{C}{O} = \frac{C^{2+} + C^{3+}}{O^{2+}} \quad (5)$$

that can be simplified to $C/O = C^{2+}/O^{2+}$ when no C IV emission is detected.

In Fig. 1, we plot the relation between total O/H and C/O for our calibration sample. The objects are identified according to their nature and the method used to derive O/H and C/O. We distinguish between objects with temperatures obtained from the [O III] 5007/1664 ratio (30), objects whose O/H was calculated using the empirical relation between O/H and t_e([O III]) given in Amorín et al. (2015) (6), and objects whose O/H and C/O were calculated using the electron temperature from the [O III]5007/1664 ratio (8). For the latter, typical errors in O/H are ∼0.18 dex, while in the two first cases they are slightly lower, ∼0.10 dex.

On average, C/O tend to increase with metallicity, as carbon is essentially a secondary element (i.e. its relative production is higher for higher O/H) mainly ejected into the interstellar medium by massive stars (e.g. Henry et al. 2000). This trend starts to be observed in our sample from 12+log(O/H) > 7.4. However, the dispersion of this relation, of about 0.25 dex, is larger than the average C/O errors (∼0.15 dex), owing to the different physical processes affecting metallicity and the ratio between a primary element as O and a secondary one as C. This is the case of hydrodynamical processes, including metal-enriched outflows or inflows of metal-poor gas, which can change metallicity and keep relatively unaffected C/O (e.g. Edmunds 1990). Other factors that could also modify this ratio are, for instance, different star formation efficiencies or the presence of a non-standard initial mass function (e.g. Gavilán, Buell & Mollá 2005; Mattsson 2010) Therefore, as no clear trend can be taken between O/H and C/O, C/O has to be previously calculated to allow the derivation of O/H abundances using carbon lines. This is similar to the situation in the optical, when N/O must be determined before deriving O/H using [N II] emission lines (Pérez-Montero & Contini 2009; Amorín, Pérez-Montero & Vílchez 2010).

3 MODEL AND METHOD DESCRIPTION

Both O/H, C/O and the ionization parameter (log U) were derived using a semi-empirical approach based on the comparison between the most representative extinction-corrected emission lines observed in the UV (Lyα 1216 Å, C IV 1549 Å, O III] 1664 Å, and C III] 1908 Å) and in the optical (Hβ 4861 Å and [O III] 5007 Å) with a large grid of photoionization models covering a wide range of values in O/H, C/O and log U.

The photoionization models were calculated using the code CLOUDY v.13.01 (Ferland et al. 2013). In all models, we adopted a spherical geometry of constant density gas (100 cm^{-3}), filling factor of 10^{-1}, and a standard gas-to-dust mass ratio around an ionizing point source with the spectral energy distribution (SED) of a 1 Myr old cluster using POPSTAR (Mollá, García-Vargas & Bressan 2009) model atmospheres at the metallicity of the gas. The calculation was stopped in each model and the lines were thus retrieved when the electron density fraction was lower than 10 per cent.

Although several authors have pointed out the importance of the assumed SED in the models for the determination of abundances (e.g. Kewley, Jansen & Geller 2005; Morisset et al. 2016), as our approach is semi-empirical it is possible to assess any systematic effect and the uncertainty associated with the assumption of an ionizing stellar cluster of a single age in our models.

The grid covers input oxygen abundances in the range [7.1, 9.1] in bins of 0.1 dex, log U in the range [−4.0, −1.5] in bins of 0.25 dex and assumes solar proportions for the rest of elements, with the exception of carbon, that takes values in the range of C/O = [−1.4, 0.6] in bins of 0.125 dex, and nitrogen, for which we assume a secondary origin and a constant solar ratio log(C/N) = 0.6 (Asplund et al. 2009). The assumption of a constant C/N ratio is justified by the expected similar behaviour between primary and secondary elements under hydrodynamical effects (e.g. Edmunds 1990) and supported by recent observations of galaxies at low (Berg et al. 2016) and high redshifts (Steidel et al. 2016), which show a constant trend in C/N with metallicity. Under the above conditions, the grid consists on a total of 3927 models that can be obtained from the 3MDB data base (Morisset, Delgado-Inglada & Flores-Fajardo 2015).[1]

A PYTHON-based routine called HII-CHI-MISTRY-UV [2] (hereafter HCM-UV was developed in order to calculate O/H, C/O and log U comparing the observed relative UV and optical emission lines with the predictions from the models. The methodology is the same as that described for the optical in Pérez-Montero (2014). In a first step, the code calculates C/O in order to constrain the space of models in which O/H abundances can be calculated using UV carbon emission lines.

The C/O abundance ratio is derived as the average of the χ^2-weighted distribution of the C/O values in the models. The χ^2 values are calculated as the relative quadratic differences between observed and model-predicted emission-line ratios sensitive to C/O. The ratio R_{O3} is used when O III] 1664 and 5007 Å are observed. In all cases, we also use the C3O3 parameter, defined as

$$C3O3 = \log\left(\frac{I(C\,III]\ 1908\ Å) + I(C\,IV\ 1549\ Å)}{I(O\,III]\ 1664\ Å)}\right), \quad (6)$$

which can be also defined in the absence of the C IV line as the ratio of the C III] and [O III] lines. As shown in Fig. 2, according to models C3O3 has little dependence on O/H, while the dependence on log U is only significant for very low excitation. Fig. 2 also shows the

[1] 3MdB project and the models can be found in https://sites.google.com/site/mexicanmillionmodels/

[2] The routine HCM-UV is publicly available at http://www.iaa.es/~epm/HII-CHI-mistry-UV.html

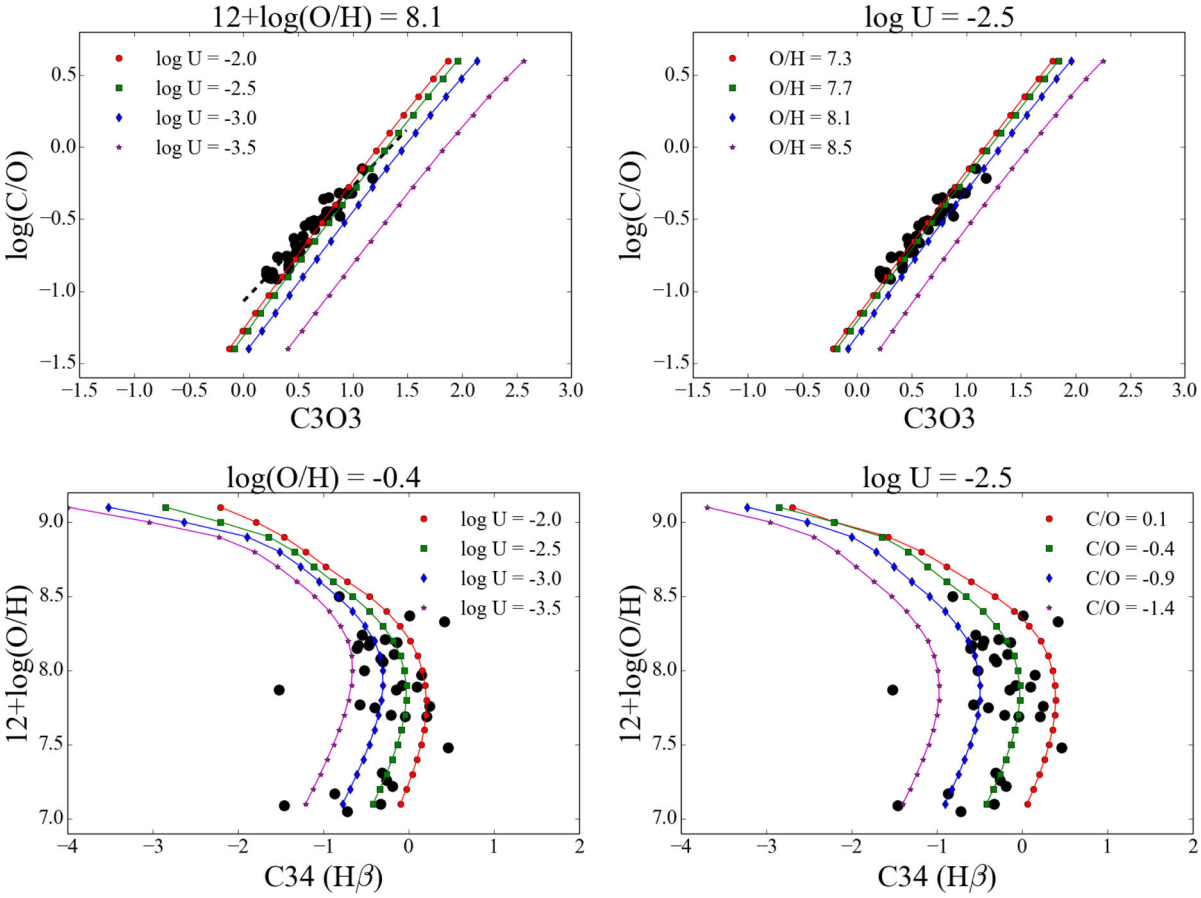

Figure 2. Relations between the relevant emission line ratios, models and derived abundances for the compiled sample. Upper panels: relation between C3O3 and C/O at fixed O/H (left) and fixed log U (right). The dashed black line represents the linear fitting to the observations. Lower panels: relation between C34 and O/H at fixed C/O (left) and at fixed log U (right).

calibration sample, which follow a linear trend that can be used to derive C/O empirically:

$$\log(\mathrm{C/O}) = -1.069 + 0.796\mathrm{C3O3} \quad (7)$$

with a dispersion of 0.20 dex, calculated as the standard deviation of the residuals.

Once C/O is fixed in the grid of models, both O/H and log U are calculated as the mean of the model input values in the χ^2-weighted distribution, where again the χ^2 values for each model are derived from the quadratic relative differences between the observed and predicted emission-line ratios sensitive to O/H and log U. Also in this case, R_{O3} is used when O III] 1664 and [O III] 5007 are observed. Similarly to the case of C/O, the χ^2 values for R_{O3} are added in quadrature to other emission-line ratios from the UV, such as the C34 parameter, defined as

$$\mathrm{C34} = \log\left(\frac{\mathrm{I(C\,III]\ 1908\ \text{Å}) + I(C\,IV1549\ \text{Å})}}{I(\mathrm{H\,I})}\right), \quad (8)$$

where I(H I) is the intensity of a hydrogen recombination line. When optical emission lines are available, the H I line is Hβ 4861 Å. As in the case of C3O3, C34 can be defined in the absence of C IV lines using only C III] lines. As shown in Fig. 2, this ratio has a very similar dependence with O/H as the R_{23} parameter (i.e. [O II]+[O III] relative to Hβ, Pagel et al. 1979) as it is double valued (i.e. it increases with O/H for low O/H and it decreases for high O/H). Besides, it presents additional dependence on log U and C/O that contribute to enlarge the dispersion. The dependence on C/O is limited in our method because C/O is constrained in the first iteration of our calculations. As shown in Fig. 2, the C34 parameter also presents a large dependence on log U. The latter is obtained in this iteration as the average value of the resulting distribution. The dependence on log U is alleviated using an additional parameter in the total χ^2 that depends on the C3C4 index, defined as the ratio between the C III] and C IV lines:

$$\mathrm{C3C4} = \log\left(\frac{\mathrm{I(C\,III]\ 1908\ \text{Å})}}{\mathrm{I(C\,IV1549\ \text{Å}}}\right). \quad (9)$$

4 RESULTS AND DISCUSSION

In Fig. 3, we show the comparison between the chemical abundances derived from both the direct method and from HCM-UV. In the two upper panels, the latter uses all the available optical (Hβ and [O III] 5007) and UV (C IV, C III], O III]) emission lines. Overall, we find a good agreement between these two data sets, both for C/O and O/H > 7.5, with a mean offset that is lower than the uncertainty of the direct method (i.e. <0.10 dex) both for O/H and C/O. The overall standard deviation of the residuals is 0.15 dex for O/H and 0.16 dex for C/O.

Interestingly, using HCM-UV it could be possible to obtain abundances from UV lines adding only follow-up observations of the blue part of the rest-frame optical spectrum corresponding to [O III]

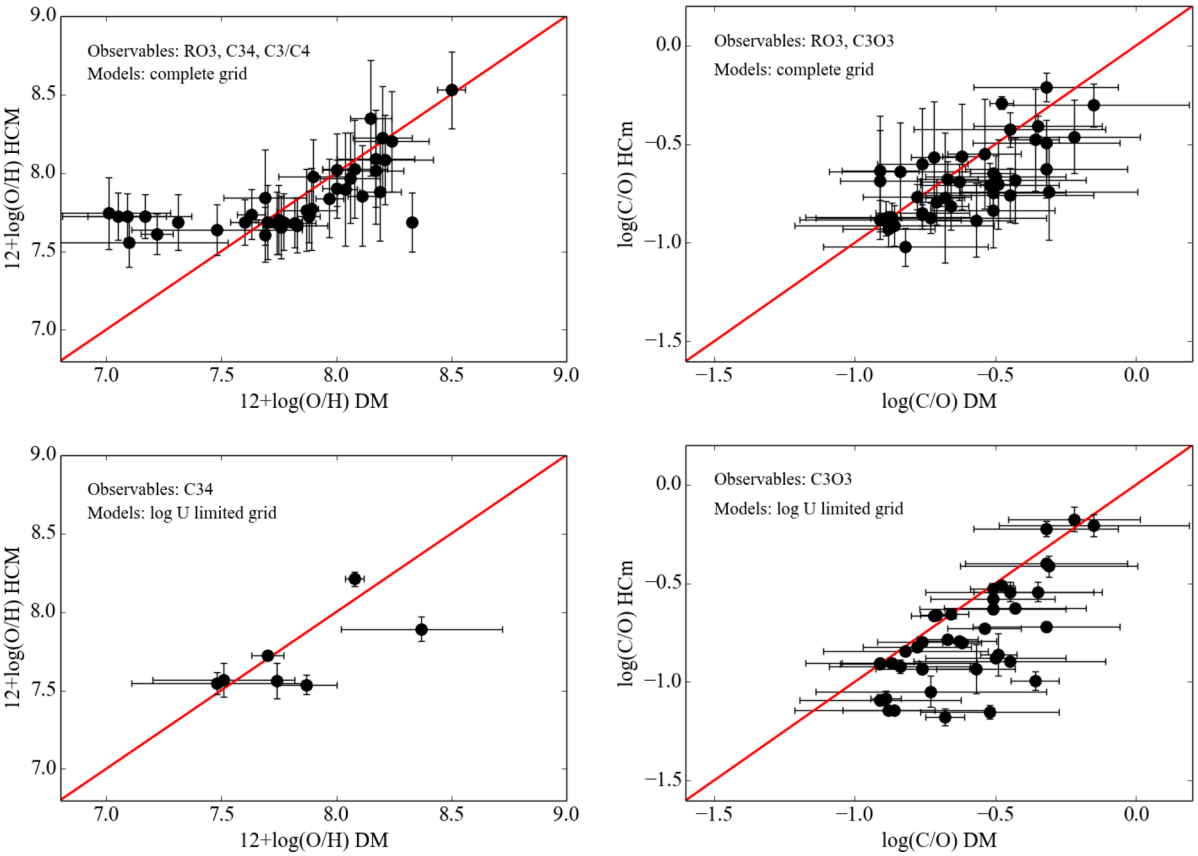

Figure 3. Comparison between C/O (right) and O/H (left) abundances derived from the direct method and from HCM-UV under different assumptions. The HCM-UV-based abundances in lower panels were derived using only UV lines, while for upper panels they also include optical information, i.e. Hβ and [O III] 5007 Å. The red solid lines represent in all cases the 1:1 relation.

5007 Å and Hβ, without any low-excitation emission line such as [O II] 3727 Å. Though for very low values of O/H ($\lesssim$7.5), the abundances derived by HCM-UV do not follow any correlation with those from the direct method, the code essentially identifies all of these objects as extremely metal-poor galaxies.

When the R_{O3} ratio – used to derive t_e([O III]) in the direct method – cannot be derived due to the absence of optical lines, the code follows the same strategy as in Pérez-Montero (2014): it constrains the grid of models by assuming an empirical law between O/H and log U in such a way that metal-poor objects have higher log U and metal-rich objects have lower log U. This empirical relation was already observed by Dopita & Evans (1986) and could be related with an evolutionary sequence. Since our sample small compared with the sample studied in Pérez-Montero (2014), we adopt the same constrain for our grid. In Fig. 4, we show the comparison between the empirical O/H–log U relation empirically derived for Sánchez Almeida et al. (2016) and Pérez-Montero et al. (2016) and the values derived for our sample using all lines. As can be seen the trend is well followed by the points.

By using this constrained grid, the code calculates C/O using only the C3O3 ratio and the same procedure as described above and then derives O/H and log U using the C3C4 and C34 parameters, but taking Lyα as the hydrogen recombination line. This approach, however, should be used with caution. The Lyα line is resonant and photons scatter in the neutral hydrogen, thus having a complex radiation transfer. Especially for faint Lyα emission (i.e. low equivalent width), this may produce an additional source of systematic uncertainty.

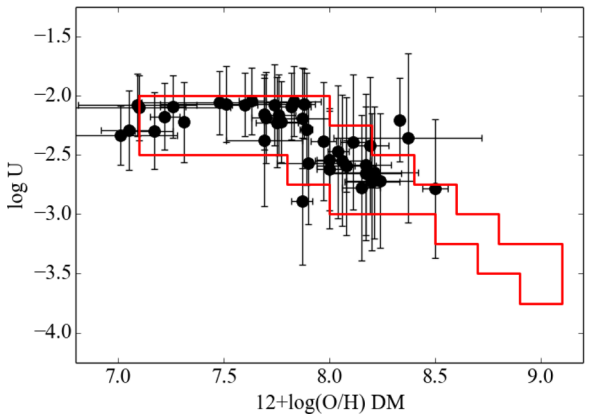

Figure 4. Relation between O/H as derived from the direct method and log U derived using HCM-UV using all available lines and the complete grid of models for the selected sample of objects. The red solid line encompasses the grid of models empirically constrained in Pérez-Montero (2014).

In the two lower panels of Fig. 3, we show the comparison between the abundances derived from the direct method and from HCM-UV in absence of the optical emission lines. The number of points with a reliable measurement of Lyα in our sample is very low, but all the objects are identified as metal poor in this sample. Regarding C/O, as this ratio has a very little dependence on the electron temperature, the agreement is still very good, i.e. the mean offset is lower than the uncertainty of the direct method and the

standard deviation of the residuals is 0.20 dex, fairly similar to that obtained using optical lines.

This result underlines the importance of the C/O abundance ratio as an indicator of the chemical content of galaxies at different epochs. Apart from the reliability of the results only using O III] and C III] UV emission lines, C/O is not affected by hydrodynamical processes, such as inflows or outflows, and can be more tightly related with other integrated properties of galaxies such as stellar mass, as in the case of N/O (Amorín et al. 2010; Pérez-Montero et al. 2013, 2016).

When no previous determination of C/O can be made (i.e. the C3O3 ratio cannot be measured), we follow again the procedure described in Pérez-Montero (2014) for the case of N/O: the code adopts a new constrain for the space of models assuming a given empirical relation between O/H and C/O to calculate O/H using the C34 parameter. The code then uses the relation between O/H and N/O shown in fig. 3 of Pérez-Montero (2014) and assumes the C/N solar ratio for all the sample.

5 CONCLUSION

In this work, we present a semi-empirical method to derive oxygen (O/H) and carbon abundances (C/O) from rest-frame UV emission lines, which are consistent with those obtained using the direct method.

We highlight the potential use of this method for (T_e-consistent) metallicity inferences at high redshifts ($z > 2$), e.g. through deep optical spectroscopy with large ground-based telescopes (Amorín et al. 2017) or using future space telescopes, such as the *JWST*. For example, the NIRSpec spectrograph onboard the *JWST*, will be able to detect the full set of rest UV and optical lines required to use this method for galaxies spanning from $z \sim 3.5$ to $z \sim 9$ in relatively short exposure times. Particularly interesting could be the use of this technique to provide metallicity constraints for primeval galaxies in the epoch of cosmic reionization (at $z > 6$). In these presumably metal-poor objects, rest UV emission lines with relatively high EWs (such as C III], C IV, and O III]) are apparently ubiquitous (e.g. Stark et al. 2015, 2017), but the access to faint key optical lines (such as [O III] 4363 Å and [O II] 3727 Å in the case of high-ionization objects) will be very limited, thus making T_e-consistent metallicity inferences extremely challenging.

ACKNOWLEDGEMENTS

We thank the anonymous referee for constructing and helpful comments. EPM acknowledges support from the Spanish MICINN through grants AYA2010-21887-C04-01 and AYA2013-47742-C4-1-P and the Junta de Andalucía for grant EXC/2011 FQM-7058. RA acknowledges the support from the ERC Advanced Grant 695671 'QUENCH' and the FP7 SPACE project 'ASTRODEEP' (Ref. No.: 312725), supported by the European Commission.

REFERENCES

Aggarwald K. M., Keenan F. P., 2004, Phys. Scr., 69, 385
Amorín R. O., Pérez-Montero E., Vílchez J. M., 2010, ApJ, 715, L128
Amorín R. et al., 2014, ApJ, 788, L4
Amorín R. et al., 2015, A&A, 578, A105
Amorín R. et al., 2017, preprint (arXiv:1701.04416)
Asplund M., Grevesse N., Sauval A. J., Scott P., 2009, ARA&A, 47, 481
Bayliss M. B., Rigby J. R., Sharon K., Wuyts E., Florian M., Gladders M. D., Johnson T., Oguri M., 2014, ApJ, 790, 144
Berg D. A., Skillman E. D., Henry R. B. C., Erb D. K., Carigi L., 2016, ApJ, 827, 126
Berrington K. A., Burke P. G., Dufton P. L., Kingston A. E., 1985, At. Data Nucl. Data Tables, 33, 195
Calzetti D., Armus L., Bohlin R. C., Kinney A. L., Koornneef J., Storchi-Bergmann T., 2000, ApJ, 533, 682
Cardelli J. A., Clayton G. C., Mathis J. S., 1989, ApJ, 345, 245
Chiappini C., Romano D., Matteucci F., 2003, MNRAS, 339, 63
Christensen L. et al., 2012, MNRAS, 427, 1973
Contini T. et al., 2016, A&A, 591, A49
de Barros S. et al., 2016, A&A, 585, A51
Dopita M. A., Evans I. N., 1986, ApJ, 307, 431
Edmunds M. G., 1990, MNRAS, 246, 678
Edmunds M. G., Pagel B. E. J., 1978, MNRAS, 185, 77P
Erb D. K., Pettini M., Shapley A. E., Steidel C. C., Law D. R., Reddy N. A., 2010, ApJ, 719, 1168
Feltre A., Charlot S., Gutkin J., 2016, MNRAS, 456, 3354
Ferland G. J. et al., 2013, Rev. Mex. Astron. Astrofis., 49, 137
Garnett D. R., Skillman E. D., Dufour R. J., Peimbert M., Torres-Peimbert S., Terlevich R., Terlevich E., Shields G. A., 1995, ApJ, 443, 64
Garnett D. R., Skillman E. D., Dufour R. J., Shields G. A., 1997, ApJ, 481, 174
Garnett D. R., Shields G. A., Peimbert M., Torres-Peimbert S., Skillman E. D., Dufour R. J., Terlevich E., Terlevich R. J., 1999, ApJ, 513, 168
Gavilán M., Buell J. F., Mollá M., 2005, A&A, 432, 861
Gutkin J., Charlot S., Bruzual G., 2016, MNRAS, 462, 1757
Henry R. B. C., Edmunds M. G., Köppen J., 2000, ApJ, 541, 660
Iglesias-Páramo J. et al., 2016, ApJ, 826, 71
Izotov Y. I., Chaffee F. H., Foltz C. B., Green R. F., Guseva N. G., Thuan T. X., 1999, ApJ, 527, 757
James B. L. et al., 2014, MNRAS, 440, 1794
Jaskot A., Ravindranath S., 2016, ApJ, 833, 136
Karman W. et al., 2015, A&A, 574, A11
Kewley L. J., Jansen R. A., Geller M. J., 2005, PASP, 117, 227
Kobulnicky H. A., Skillman E. D., 1998, ApJ, 497, 601
Kobulnicky H. A., Skillman E. D., Roy J.-R., Walsh J. R., Rosa M. R., 1997, ApJ, 477, 679
Kurk J. et al., 2013, A&A, 549, A63
Kurt C. M., Dufour R. J., Garnett D. R., Skillman E. D., Mathis J. S., Peimbert M., Torres-Peimbert S., Walter D. K., 1995, Rev. Mex. Astron. Astrofis. Ser. Conf., 3, 223
Le Fèvre O. et al., 2015, A&A, 576, A79
Lilly S. J. et al., 2007, ApJS, 172, 70
Luridiana V., Morisset C., Shaw R. A., 2012, in Manchado A., Stanghellini L., Schönberner D., eds, Proc. IAU Symp. 283, Planetary Nebulae: An Eye to the Future. Cambridge Univ. Press, Cambridge, p. 422
Maseda M. V. et al., 2014, ApJ, 791, 17
Mattsson L., 2010, A&A, 515, A68
Mollá M., García-Vargas M. L., Bressan A., 2009, MNRAS, 398, 451
Morisset C., Delgado-Inglada G., Flores-Fajardo N., 2015, Rev. Mex. Astron. Astrofis., 51, 103
Morisset C. et al., 2016, A&A, 594, A37
Onodera M. et al., 2016, ApJ, 822, 42
Pagel B. E. J., Edmunds M. G., Blackwell D. E., Chun M. S., Smith G., 1979, MNRAS, 189, 95
Patrício V. et al., 2016, MNRAS, 456, 4191
Pérez-Montero E., 2014, MNRAS, 441, 2663
Pérez-Montero E., Contini T., 2009, MNRAS, 398, 949
Pérez-Montero E. et al., 2013, A&A, 549, A25
Pérez-Montero E. et al., 2016, A&A, 595, A62
Sánchez Almeida J., Pérez-Montero E., Morales-Luis A. B., Muñoz-Tuñón C., García-Benito R., Nuza S. E., Kitaura F. S., 2016, ApJ, 819, 110
Sanders R. L. et al., 2016, ApJ, 825, L23
Shapley A. E., Steidel C. C., Pettini M., Adelberger K. L., 2003, ApJ, 588, 65
Shapley A. E. et al., 2015, ApJ, 801, 88
Stark D. P. et al., 2014, MNRAS, 445, 3200
Stark D. P. et al., 2015, MNRAS, 450, 1846

Stark D. P. et al., 2017, MNRAS, 464, 469
Steidel C. C., Adelberger K. L., Shapley A. E., Pettini M., Dickinson M., Giavalisco M., 2003, ApJ, 592, 728
Steidel C. C. et al., 2014, ApJ, 795, 165
Steidel C. C., Strom A. L., Pettini M., Rudie G. C., Reddy N. A., Trainor R. F., 2016, ApJ, 826, 159
Thuan T. X., Izotov Y. I., Foltz C. B., 1999, ApJ, 525, 105
Trainor R. F., Strom A. L., Steidel C. C., Rudie G. C., 2016, ApJ, 832, 171
Troncoso P. et al., 2014, A&A, 563, A58
Vanzella E. et al., 2016a, ApJ, 821, L27
Vanzella E. et al., 2016b, ApJ, 825, 41
Vanzella E. et al., 2017, MNRAS, 465, 3803
Villar-Martín M., Cerviño M., González Delgado R. M., 2004, MNRAS, 355, 1132

This paper has been typeset from a TEX/LATEX file prepared by the author.